arXiv:1703.04716v1 [cond-mat.supr-con] 2 Mar 2017

# Single-gap superconductivity in doped $SrTiO_3$

Markus Thiemann[1*†], Manfred H. Beutel[1*], Martin Dressel[1], Nicholas R. Lee-Hone[2], David M. Broun[2,3], Evangelos Fillis-Tsirakis[4], Hans Boschker[4], Jochen Mannhart[4] and Marc Scheffler[1,†]

[1] *1. Physikalisches Institut, Universität Stuttgart, D-70569 Stuttgart, Germany*

[2] *Department of Physics, Simon Fraser University, Burnaby, BC, V5A 1S6, Canada*

[3] *Canadian Institute for Advance Research, Toronto, Ontario, MG5 1Z8, Canada*

[4] *Max Planck Institute for Solid State Research, D-70569 Stuttgart, Germany*

[*] *These authors contributed equally to this work*

[†] *Correspondence to:*

*markus.thiemann@pi1.physik.uni-stuttgart.de, scheffl@pi1.physik.uni-stuttgart.de*

**Doped $SrTiO_3$ is a superconducting oxide that features one of the lowest charge carrier densities among all known superconductors. Undoped, semiconducting $SrTiO_3$ exhibits three unoccupied electronic bands, which can be filled successively by doping, making this system an ideal candidate for multiband superconductivity[1–4]. The increase of charge carrier density is accompanied by the evolution of a superconducting dome in the phase diagram with critical temperature $T_c$ of up to 0.4 K [5,6]. Despite a long-running interest in the superconducting properties of doped $SrTiO_3$, many aspects concerning its possible multiband superconductivity remain enigmatic. Here we use microwave spectroscopy[7] to determine the complete electrodynamic response of superconducting Nb-doped $SrTiO_3$. Surprisingly we find that**

**our data can be fully explained in terms of single-gap BCS superconductivity. From our resonant microwave measurements[7,8] at temperatures 0.07 K - 0.4 K and frequencies 2 GHz - 23 GHz, we obtain the optical conductivity for five different samples with charge carrier concentrations between $0.3 \times 10^{20}$ cm$^{-3}$ and $2.3 \times 10^{20}$ cm$^{-3}$. This GHz conductivity gives us information on both the quasiparticles and the superconducting condensate, and we determine the temperature dependence of the superfluid density and the energy gap $2\Delta$. Despite significant deviations from single-gap behavior being expected for doped $SrTiO_3$, our data can be described with a single gap with a coupling ratio of $2\Delta_0/k_BT_c \approx 3.5$ for all carrier concentrations. Therefore we conclude that doped $SrTiO_3$ is a single-gap superconductor that can be described by standard BCS theory although not being within the Migdal limit[9].**

$SrTiO_3$ is remarkable in many ways. At the stoichiometric composition it is a band insulator with a dielectric constant that increases by two orders of magnitude on cooling due to proximity to a ferroelectric instability[10]. Its polar nature is a key ingredient for the (super-)conducting interface between $SrTiO_3$ and $LaAlO_3$[11,12] and is also thought to be important to 100 K superconductivity in monolayers of FeSe grown on $SrTiO_3$[13]. The electronic structure of $SrTiO_3$ contains three bands, originating from the $t_{2g}$ orbitals of the titanium ion, which can be filled with charge carriers successively upon doping[2]. This results in a Fermi energy, $E_F$, that is small compared to the Debye energy, leading to a breakdown of the Migdal regime of adiabatic electron-phonon interaction, in which BCS theory was derived[9,14]. In 1964 Schooley *et al.*[15] discovered Nb-doped $SrTiO_3$ to be the first example of a superconducting oxide. Upon changing the doping level and thus the charge carrier concentration, the transition temperature exhibited the first-known example

of a "superconducting dome", with a maximum $T_c$ of 0.4 K[5]. Since then, the underlying physics of superconducting domes, found for numerous materials classes, has been the subject of intense study[16–20]. Furthermore, the electronic structure of $SrTiO_3$, with multiple bands crossing the Fermi level, makes it a strong candidate for exploring multiband superconductivity in a tunable manner. Indeed, indications for multiband superconductivity were found in early tunneling measurements[1] and, more recently, in thermal conductivity measurements in magnetic field[21].

In order to explore the superconducting charge dynamics of Nb-doped $SrTiO_3$, we have performed microwave measurements over a frequency range of $\omega/2\pi = 2$ to 23 GHz and a temperature range of $T = 0.07$ to 0.4 K, smoothly crossing from $\hbar\omega \ll k_B T$ to $\hbar\omega \gg k_B T$ and thereby covering all the energy scales relevant for superconductivity. This broad range of frequencies and temperatures is accessed using stripline resonators with a Nb-doped $SrTiO_3$ sample acting as a ground plane[7,8], as shown schematically in Fig. 1**a**. The measured bandwidth $\nu_{\rm B}$ of the resonances is related to the surface resistance of the sample via cavity perturbation theory (see supplementary material). Accordingly a sharp drop in $\nu_{\rm B}$ is visible when the sample turns superconducting, as illustrated in Fig. 1**c**. The transition temperature $T_{\rm c}$ was obtained from $\nu_{\rm B}$ at the lowest resonator frequency in order to be as close as possible to the DC limit. In Fig. 1**b** we plot the variation of $T_c$ measured in this manner as a function of doping level, and our data fit well within the literature reports of this superconducting dome, which are included for comparison[1,3,6].

From the microwave surface impedance $\hat{Z}_{\rm s}$ we determine the complex optical conductivity $\hat{\sigma} = \sigma_1 + {\rm i}\sigma_2$, allowing us to probe both the quasiparticles and the superfluid. $\sigma_1$ represents the microwave losses in the sample and therefore is a measure for the energy absorption rate. One contri-

bution $\sigma_1^{\rm th}$ stems from thermally excited quasiparticles, which provide the only possible absorption process in a superconductor at frequencies below the superconducting gap, $2\Delta$ [22]. The other contributing process, $\sigma_1^{\rm ph}$, is the breaking of Cooper pairs by photons, thus generating quasiparticles by direct optical excitation across the superconducting energy gap. The latter process can only occur for frequencies $\hbar\omega > 2\Delta$, in contrast to $\sigma_1^{\rm th}$. Therefore, the total conductivity spectrum $\sigma_1(\omega) = \sigma_1^{\rm th}(\omega) + \sigma_1^{\rm ph}(\omega)$ exhibits a kink at $\hbar\omega = 2\Delta$. The appearance of this behaviour in $\sigma$ allows the energy gap to be inferred directly from the microwave data, for instance in the frequency spectra shown in Fig. 2**b** for a sample with charge carrier concentration $n = 1.7 \times 10^{20}$ cm$^{-3}$, which are in accord with the theoretical Mattis-Bardeen predictions[22,23]. In fact, this close correspondence is our first indication that Nb-doped $SrTiO_3$ can be understood within a single-gap BCS picture. The frequency at which the kinks occur in $\sigma_1(\omega)$ as well as in $\sigma_2(\omega)$, marks the size of the energy gap $2\Delta$ at this temperature[22]. (Note that the kinks in $\sigma_2(\omega)$ are unique to the Mattis–Bardeen limit in which the scattering rate $\Gamma > 2\Delta/\hbar$, indicating a superconductor in the dirty limit.) By simultaneously fitting the Mattis-Bardeen equations to $\sigma_1(\omega)$ and $\sigma_2(\omega)$ at various temperatures, we determine the temperature dependence of the energy gap $2\Delta(T)$ for the samples with $n = 1.2 \times 10^{20}$ cm$^{-3}$ and $n = 1.7 \times 10^{20}$ cm$^{-3}$, as shown as open symbols in Fig. 4**a**, with extremely fine temperature resolution.

An independent way to extract $2\Delta(T)$ from our data, without relying on Mattis-Bardeen theory in detail, is by analyzing the temperature dependence of $\sigma_1$ for a set of frequencies, namely the resonator harmonics that we have available. For any given frequency $\omega$ that is smaller than the zero-temperature energy gap $2\Delta_0$, the temperature-dependent $\sigma_1(T)$ will indicate pronounced ad-

ditional losses due to Cooper-pair breaking as the temperature is scanned through the point at which $2\Delta(T)$ falls below $\hbar\omega$. This is evident as kinks in $\sigma_1(T)$ in Fig. 3**a**, which shows data for the $n = 1.7 \times 10^{20}$ cm$^{-3}$ sample for seven different resonator frequencies. The temperature dependence of the energy gap inferred by this method is plotted as the stars in the frequency-temperature plane of Fig. 3**a**.

The complete set of $2\Delta(T)$ is shown for all five samples in Fig. 4**a**. The data are well fit by the temperature dependence of $2\Delta$ predicted for a single-gap BCS superconductor[14] where we leave the ratio $2\Delta_0/k_{\rm B}T_{\rm c}$ as fit parameter. The resulting values for $2\Delta_0/k_{\rm B}T_{\rm c}$ for the different concentrations, as shown in Fig. 4**a**, are consistent with the BCS prediction for weak-coupling superconductivity, $2\Delta_0/k_{\rm B}T_{\rm c} \approx 3.5$ [14]. This value is in line with recent tunneling results for doped $SrTiO_3$ thin films[9]. From our evaluation of the microwave losses, which are caused by thermal quasiparticles and by breaking of Cooper pairs, a surprisingly robust picture of single-gap superconductivity emerges.

To obtain further insight into the superconducting charge dynamics we turn to the electrodynamic response of the Cooper pair condensate, which governs the superconducting penetration depth. For temperatures below $T_{\rm c}$ and at low frequencies, the out-of-phase part of the conductivity, $\sigma_2$, is dominated by the superfluid response. We define the superfluid density as

$$n_{\rm s}(T) \equiv \frac{1}{\lambda^2} = \lim_{\omega \to 0} \omega \mu_0 \sigma_2(\omega, T) \ , \tag{1}$$

where $\lambda$ is the London penetration depth[14]. In practice we discuss the normalized superfluid density $\rho_s(T) = n_{\rm s}(T)/n_{\rm s}(T = 0)$, which we obtain from our lowest measurement frequency, $\omega/2\pi \approx 2$ GHz. The resulting temperature dependence of the superfluid density $\rho_{\rm s}(T)$ is shown

in Fig. 3**b** for the sample with a charge carrier concentration of $n = 1.7 \times 10^{20}$ cm$^{-3}$. Previous studies on multiband superconductors have revealed characteristic features in $\rho_{\rm s}(T)$ such as a kink for $V_3Si$[25] or the presence of small activation energies in $MgB_2$[26] and FeSe[27]. In our data on Nb-doped $SrTiO_3$ clear signs of multi-gap behaviour are absent. Instead, our data are well described by the predictions of single-gap BCS theory, as shown in Fig. 3**b**, if the scattering rate $\Gamma$ amounts to a value at least a few times larger than $2\Delta_0/\hbar$.

We now place the microwave data into the context of other measurements on Nb-doped $SrTiO_3$ and point out some advantages of our measurement technique, which so far has not been applied to $SrTiO_3$ and might prove as an important tool for future studies of other superconductors with $T_c$ in the sub-K regime. Due to the substantial microwave probing depth, which below $T_c$ amounts to the superconducting penetration depth, one obtains information about the superconducting bulk whereas tunneling measurements probe the sample surface. Our microwave technique is contactless and has very little restrictions concerning possible samples to be studied, except for the sample size (which should be several millimeters). As with any spectroscopy, we obtain direct information about relevant energy scales such as the superconducting gap. Finally, we can address three distinct aspects of a superconductor, namely the superconducting condensate, its single-particle excitation (generation of quasiparticles by breaking of Cooper pairs), and the thermal quasiparticles, by using a single experimental technique. These particular aspects of microwave spectroscopy we would like to combine with the merits of other established techniques to reach a comprehensive understanding of the superconductivity in $SrTiO_3$.

Here we comment on recent experiments on field-dependent thermal conductivity, $\kappa(B)$, which

detect two distinct field scales, suggesting a multiband interpretation[21]. We have performed microwave measurements in magnetic field, and observe similar features (see supplementary material). However, field dependence in the vortex state is not a direct probe of energy gap, but a probe of length scales, via the magnetic length $\ell_B = \sqrt{\hbar/2eB}$, a measure of the average spacing between vortices. In a multiband superconductor, kinks in $\kappa(B)$ are expected to occur when $\ell_B$ is comparable to the band-specific coherence lengths, $\xi_{0,i} \equiv \hbar v_{F,i}/\pi\Delta_i$ in the clean limit or $\xi_i = \sqrt{\Lambda_i \xi_{0,i}}$ in the dirty limit. Here the $v_{F,i}$ are the band-specific Fermi velocities and $\Lambda_i$ the mean free paths[14]. Our strong evidence for single-gap superconductivity is consistent with multiple field scales: one interpretation is that multiple coherence lengths arise from the electronic bands having different Fermi velocities and mean free paths. Differences in Fermi velocity are consistent with results of Shubnikov-de Haas studies[3].

The crucial outstanding question is then why superconductivity in a known multiband material is so well described by single-gap BCS theory. In fact, clues to one possible answer are present in the microwave data, in particular the high degree to which the $\sigma_2(\omega)$ spectra conform to Mattis–Bardeen theory, which is a model of superconductivity in the dirty limit, $\hbar\Gamma > 2\Delta$. In this regime, it is well known from Anderson's theory of dirty superconductors that nonmagnetic scattering does not destroy superconductivity, but simply homogenizes the energy gap over the Fermi surface[28]. These ideas are confirmed by the close correspondence of the measured superfluid density with dirty-limit single-gap theory, as shown in Fig. 3**b**. They are also consistent with optical studies that suggest a Drude relaxation rate that is rather low but still higher than the superconducting energy gap that we observe[29], and a recent study of the lower critical field also highlights the role

of clean and dirty limits for superconducting $SrTiO_3$[24]. Therefore, our picture of the superconductivity in $SrTiO_3$ is that there are at least two bands contributing to the superfluid density making it a "multiband" superconductor but, due to substantial impurity scattering and Anderson's theorem, any multi-gap structure that would be present in the "clean" material is averaged out, leaving Nb-doped $SrTiO_3$ a "single-gap" superconductor. Furthermore, this archetypal BCS behaviour is observed in a material that lies outside the Migdal regime of adiabatic electron–phonon interaction. regime: However, our consistent results from both superfluid and quasiparticle response allow us to interpret doped $SrTiO_3$ as superconductor with a single BCS gap.

**Methods** The mK-measurements on Nb-doped $SrTiO_3$ were performed using superconducting stripline resonators[8,30] as schematically shown in Fig. 1**a**, which were mounted in a $^3$He/$^4$He dilution refrigerator[7]. The resonators are formed by a superconducting center conductor sandwiched between two 127$\mu$m thick sapphire plates and two superconducting ground planes. This stripline is turned into a resonant structure by adding two gaps in the center conductor, which define the length and thus the frequencies of the microwave resonator. One of the ground planes is the sample of interest, whereas the other superconducting elements are made of Pb. Given that the $T_{\rm c}$ of the sample is much lower compared to $T_{\rm c} = 7.2{\rm K}$ of the Pb resonator, the measured signal at temperatures below 1 K, i.e. the change in resonance frequency $\nu_0$ and bandwidth $\nu_{\rm B}$, is fully determined by the microwave response of the sample, and the resonator itself constitutes only a temperature-independent background[7,8]. Spectra of the relative transmission factor $S_{21}$ were measured with a vector network analyzer (VNA), showing resonance peaks at the fundamental frequency and the

higher harmonics. $\nu_0$ and $\nu_\mathrm{B}$ were obtained by fitting a complex transmission model to the $S_{21}$ spectra[32]. The complex surface impedance $\hat{Z}_\mathrm{s} = R_\mathrm{s} + \mathrm{i}X_\mathrm{s}$ is determined from changes in $\nu_0$ and $\nu_\mathrm{B}$ using the cavity perturbation approximation $\Delta\hat{Z}_\mathrm{s} = \gamma(\Delta\nu_\mathrm{B}/2 - \mathrm{i}\Delta\nu_0)$, where $\gamma$ is a structural constant depending only on the resonator geometry. Under the premise of local electrodynamics in the normal state and the scattering rate $\Gamma \gg \omega$, the complex conductivity $\hat{\sigma} \propto -\mathrm{i}\omega/\hat{Z}_\mathrm{s}^2$ can be computed by performing a $R_\mathrm{s}$-$X_\mathrm{s}$ matching in the normal state $T > T_\mathrm{c}$[31]. In this work we focus on the normalized conductivity, $\sigma_1/\sigma_\mathrm{n}$ and $\sigma_2/\sigma_\mathrm{n}$, with normal state conductivity $\sigma_\mathrm{n}$, as absolute values would require additional assumptions in the analysis and all our conclusions can be drawn from these relative changes in $\sigma$. More details about the samples, the measurements, and the data analysis are presented in the supplementary material.

**Acknowledgments** We thank G. Untereiner for resonator and sample preparation and K. Behnia and H. Y. Hwang for helpful discussions. Financial support by Carl-Zeiss-Stiftung (M.T.), DFG, and DAAD is thankfully acknowledged. D.M.B and N.R.L.H gratefully acknowledge financial support from the Natural Science and Engineering Research Council of Canada and the Canadian Institute for Advanced Research.

**Competing Interests** The authors declare that they have no competing financial interests.

**Author Contributions** M.T. and M.H.B. performed the microwave measurements and data analysis. M.S. directed the project. All coauthors contributed to the interpretation. M.T., M.H.B., and M.S. wrote the manuscript with input from all coauthors.

**Correspondence** Correspondence and requests for materials should be addressed to M. Scheffler. (email: scheffl@pi1.physik.uni-stuttgart.de).

1. Binnig, G., Baratoff, A., Hoenig, H. E. & Bednorz J. G. Two-Band Superconductivity in Nb-Doped $SrTiO_3$. *Phys. Rev. Lett.* **45**, 1352-1355 (1980).

2. van der Marel, D., van Mechelen, J. L. M. & Mazin, I. I. Common Fermi-liquid origin of $T^2$ resistivity and superconductivity in $n$-type $SrTiO_3$. *Phys. Rev. B.* **84,** 205111 (2011).

3. Lin, X. *et al.* Critical Doping for the Onset of a Two-Band Superconducting Ground State in $SrTiO_{3-\delta}$. *Phys. Rev. Lett.* **112,** 207002 (2014).

4. Lin, X., Fauqué, B. & Behnia, K. Scalable $T^2$ resistivity in a small single-component Fermi surface. *Science* **349,** 945-948 (2015).

5. Schooley, J. F. *et al.* Dependence of the Superconducting Transition Temperature on Carrier Concentration in Semiconducting $SrTiO_3$. *Phys. Rev. Lett.* **14,** 305-307 (1965).

6. Koonce, C. S., Cohen, M. L., Schooley, J. F., Hosler, W. R. & Pfeiffer, E. R. Superconducting Transition Temperatures of Semiconducting $SrTiO_3$. *Phys. Rev.* **163,** 380-390 (1967).

7. Scheffler, M. *et al.* Broadband Corbino spectroscopy and stripline resonators to study the microwave properties of superconductors. *ACTA IMEKO* **4,** 47 (2015)

8. Hafner, D., Dressel, M. & Scheffler, M. Surface-resistance measurements using superconducting stripline resonators. *Rev. Sci. Instrum.* **85,** 014702 (2014)

9. Swartz, A. G. *et al*. Strong polaronic behavior in a weak coupling superconductor. *arXiv:1608.05621*

10. Müller, K. A. & Burkard, H. $SrTiO_3$: An intrinsic quantum paraelectric below 4 K. *Phys. Rev. B* **19,** 3593-3602 (1979).

11. Ohtomo, A. & Hwang, H. Y. A high-mobility electron gas at the $LaAlO_3/SrTiO_3$ heterointerface. *Nature* **427,** 423-426 (2004).

12. Reyren, N. *et al.* Superconducting Interfaces Between Insulating Oxides. *Science* **317,** 1196-1199 (2007).

13. Zhou, Y., Millis, A. J. Charge transfer and electron-phonon coupling in monolayer FeSe on Nb-doped $SrTiO_3$. *Phys. Rev. B* **93**, 224506 (2016).

14. Tinkham, M., *Introduction to Superconductivity*, 2nd ed. (McGraw-Hill, New York, 1996).

15. Schooley, J. F., Hosler, W. R. & Cohen, M. L. Superconductivity in Semiconducting $SrTiO_3$. *Phys. Rev. Lett.* **12,** 474-475 (1964)

16. Mathur, N. D. *et al.* Magnetically mediated superconductivity in heavy fermion compounds. *Nature* **394,** 39-43 (1998)

17. Broun, D. M. What lies beneath the dome? *Nature Physics* **4,** 170-172 (2008)

18. Richter, C. *et al.* Interface superconductor with gap behaviour like a high-temperature superconductor. *Nature* **502,** 528-531 (2013)

19. Shibauchi, T, Carrington, A. & Matsuda, Y. A quantum critical point lying beneath the superconducting dome in iron pnictides. *Ann. Rev. Condens. Matter Phys.* **5,** 113 (2014)

20. Pracht, U. S. *et al.* Enhanced Cooper pairing versus suppressed phase coherence shaping the superconducting dome in coupled aluminum nanograins. *Phys. Rev. B* **93,** 100503 (2016)

21. Lin, X. *et al.* Multiple nodeless superconducting gaps in optimally doped $\mathrm{SrTi_{1-x}Nb_xO_3}$. *Phys. Rev. B* **90,** 140508 (2014)

22. Pracht, U. S. *et al.* Electrodynamics of the Superconducting State in Ultra-Thin Films at THz Frequencies, *IEEE Trans. THz Sci. Technol.* **3,** 269 (2013)

23. Mattis, D. C. & Bardeen, J. Theory of the Anomalous Skin Effect in Normal and Superconducting Metals. *Phys. Rev.* **111,** 412-417 (1958)

24. Collignon, C., Fauqué, B., Cavanna, A., Gennser, U., Mailly, D. & Behnia, K. Superfluid density and carrier concentration across a superconducting dome: the case of $\mathrm{SrTi_{1-x}Nb_xO_3}$. preprint

25. Nefyodov, Y. A., Shuvaev, A. M. & Trunin, M. R. Microwave response of $V_3Si$ single crystals: Evidence for two-gap superconductivity. *EPL (Europhysics Letters)* **72,** 638 (2005)

26. Fletcher, J. D., Carrington, A., Taylor, O. J., Kazakov, S. M. & Karpinski, J. Temperature-Dependent Anisotropy of the Penetration Depth and Coherence Length of $\mathrm{MgB_2}$. *Phys. Rev. Lett.* **95,** 097005 (2005)

27. Li, M., Lee-Hone, N. R., Chi, S., Liang, R., Hardy, W. N., Bonn, D. A., Girt, E., Broun & D. M. Superfluid density and microwave conductivity of FeSe superconductor: ultra-long-lived quasiparticles and extended s-wave energy gap. *New J. Phys* **18**, 082001 (2016)

28. Anderson, P.W. Theory of dirty Superconductors. *J. Phys. Chem. Solids* **11**, 26 (1959)

29. van Mechelen, J. L. M., van der Marel, D., Grimaldi, C., Kuzmenko, A. B., Armitage, N. P., Reyren, N., Hagemann, H. & Mazin, I. I. Electron-Phonon Interaction and Charge Carrier Mass Enhancement in $SrTiO_3$. *Phys. Rev. Lett.* **100**, 226403 (2008)

30. Scheffler, M. *et al.* Microwave spectroscopy on heavy-fermion systems: Probing the dynamics of charges and magnetic moments. *Phys. Status Solidi B* **250,** 439 (2013)

31. Dressel, M. & Grüner, G. *Electrodynamics of Solids* (Cambridge University Press, Cambridge, 2002)

32. Huttema, W. A., Morgan, A., Turner, P. J., Hardy W. N., Zhou, X., Bonn, D. A., Liang, R. & Broun, D. M. Apparatus for high-resolution microwave spectroscopy in strong magnetic fields. *Rev. Sci. Instrum.* **77,** 023901 (2006)

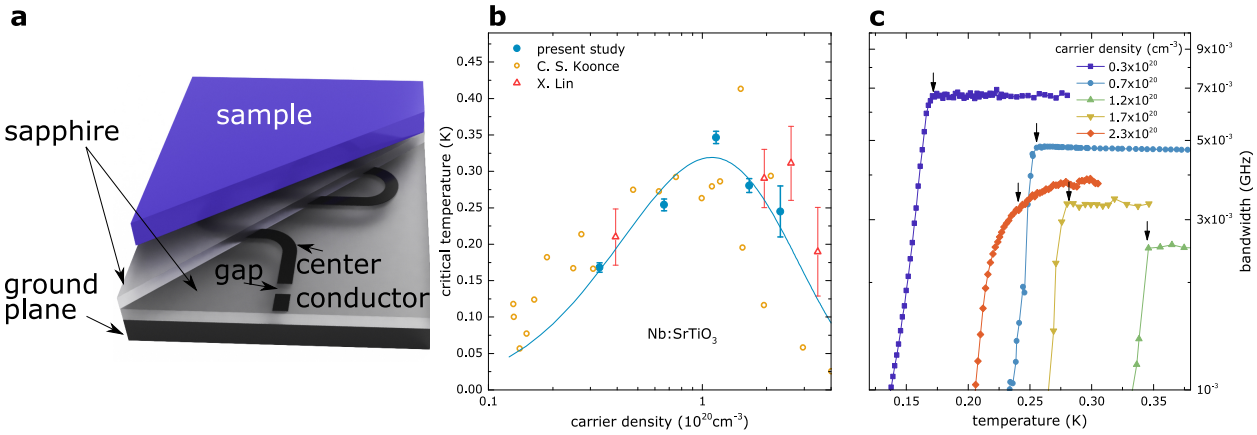


Figure 1: **a** Schematic layout of a stripline resonator. **b** Dependence of the critical temperature $T_c$ on the doping level of $SrTiO_3$, as determined from the sharp drop in the bandwidth shown in **c**. The data plotted as yellow circles and red triangles were taken from C. S. Koonce *et al.*[6] and X. Lin *et al.*[3], respectively. The solid line is a guide to the eye. **c** $T_c$ was determined from the sharp drop (indicated by arrow) in the bandwidth measured at a resonator frequency of about 2 GHz.

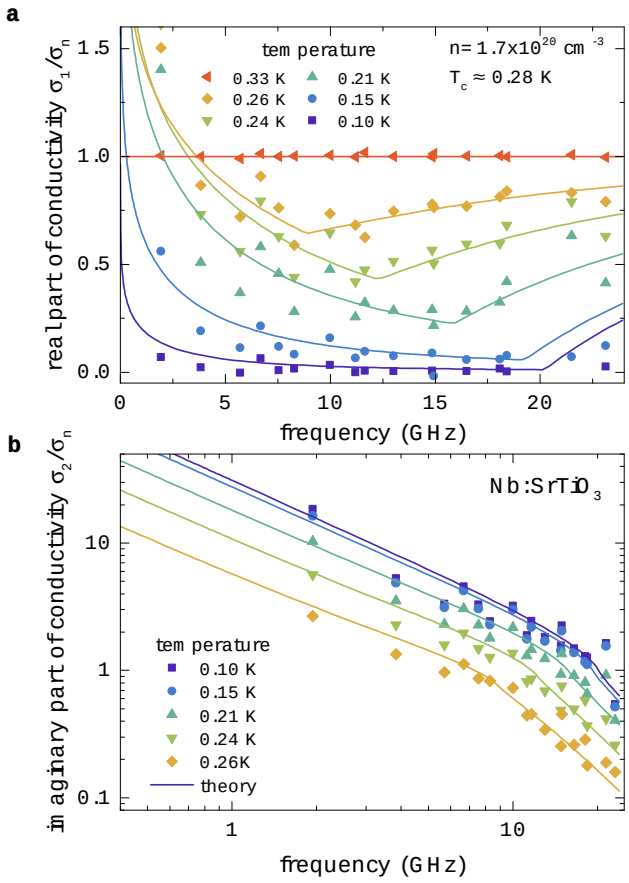


Figure 2: Frequency dependence of the complex optical conductivity $\hat{\sigma} = \sigma_1 + \mathrm{i}\sigma_2$ of superconducting Nb-doped $SrTiO_3$ with charge carrier density of $n = 1.7 \times 10^{20}\mathrm{cm}^{-3}$ and critical temperature $T_c \approx 0.28$ K plotted for different temperatures. The energy gap $2\Delta(T)$ is clearly visible as a kink in the real part $\sigma_1$ of the optical conductivity. Both the real and imaginary parts can be described well within the single-gap BCS theory at all temperatures, as represented by the solid lines. From these Mattis-Bardeen fits we obtain the energy gap $2\Delta$ for each temperature, plotted as open symbols in Fig. 4 **a**.

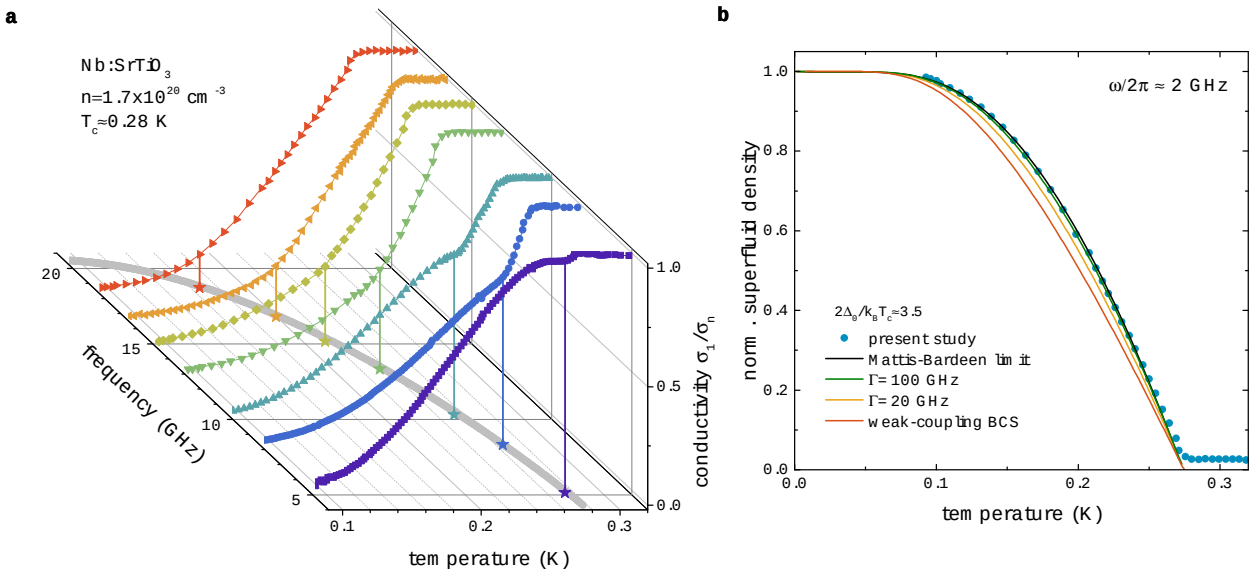


Figure 3: **a** Temperature dependence of the real part $\sigma_1$ of the optical conductivity, for various frequencies measured on Nb-doped $SrTiO_3$ with charge carrier concentration $n = 1.7 \times 10^{20}$ cm$^{-3}$. The kinks in $\sigma_1(T)$, marked by the lines projecting down to the temperature-frequency plane, indicate the crossing of the energy gap. The resulting temperature dependence of the energy gap, $2\Delta(T)$, indicated by the stars, is fully consistent with the single-band BCS prediction (grey line). **b** Temperature dependence of the normalized superfluid density $\rho_s$, as calculated from $\sigma_2$. The red and black lines are calculations according to the weak-coupling BCS and Mattis-Bardeen limits, respectively. The yellow and green lines show how the temperature dependence of the superfluid density is changed as the scattering rate $\Gamma$ is increased. All calculations assume $2\Delta_0/k_BT_c = 3.5$.

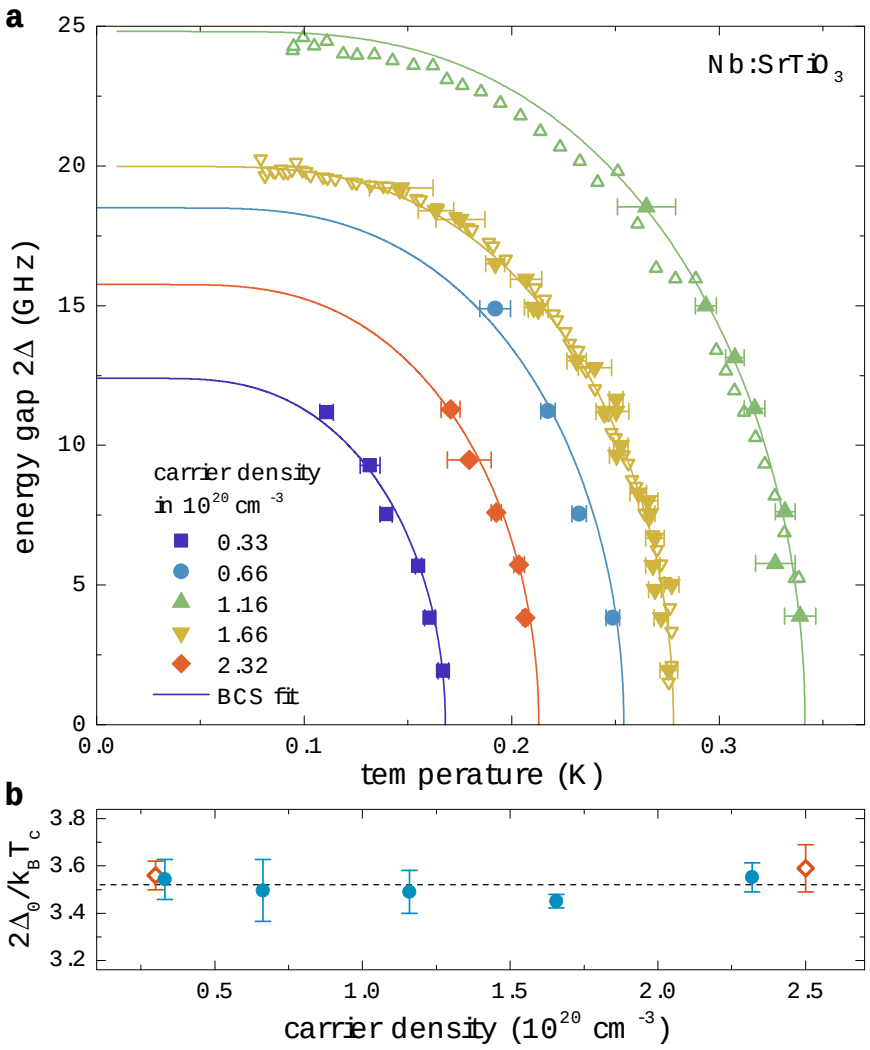


Figure 4: **a** Temperature dependence of the energy gap $2\Delta$, obtained from the temperature dependence of the real part $\sigma_1$ of the optical conductivity (filled symbols) or from fitting the Mattis-Bardeen equations to the conductivity spectra (open symbols). The solid lines indicate the temperature dependence of a single BCS gap, which was fitted to the filled-symbol data (with $\Delta_0$ as only fit parameter). **b** Resulting gap-to-$T_c$ ratio $2\Delta_0/k_BT_c$ for different carrier densities (full symbols). Open diamonds indicate data obtained by Swartz *et al.* using tunneling spectroscopy on thin films[9].